CMS Physics Analysis Summary

Contact: cms-pag-conveners-exotica@cern.ch 2014/07/10

Search for Pair-production of First Generation Scalar Leptoquarks in pp Collisions at $\sqrt{s}$ = 8 TeV

The CMS Collaboration

Abstract

A search for pair-production of first generation scalar leptoquarks is performed in the final states containing two electrons and at least two jets or an electron, a neutrino, and at least two jets using proton-proton collision data at $\sqrt{s} = 8$ TeV. The data were collected by the CMS detector at the LHC, corresponding to an integrated luminosity of 19.6 fb^{-1}. First generation scalar leptoquarks with masses less than 1005 (845) GeV are excluded for $\beta = 1(0.5)$, where β is the branching fraction of a leptoquark to a charged lepton and a quark. These limits are the most stringent limits on first generation leptoquarks to date.

1 Introduction

The structure of the standard model (SM) of particle physics suggests a fundamental relationship between quarks and leptons. In some theories beyond the SM, such as SU(5) grand-unification [1], Pati-Salam SU(4) [2], composite models [3], technicolor [4–6], and superstring-inspired E_6 models [7], the existence of a new symmetry relates the quarks and leptons in a fundamental way.

These models predict the existence of new bosons, called leptoquarks. The leptoquark (LQ) is colored, has fractional electric charge, can be either a scalar or vector particle, and couples to a lepton and a quark with coupling strength λ. The leptoquark decays to a charged lepton and a quark, with unknown branching fraction, β, or a neutrino and a quark, with branching fraction $(1-\beta)$.

A review of LQ phenomenology and searches can be found in Refs. [8, 9]. Constraints from experiments sensitive to flavor-changing neutral currents, lepton-family-number violation, and other rare processes favor LQs that couple to quarks and leptons within the same SM generation, for LQ masses accessible to current colliders [10]. The dominant mechanisms for the production of LQ pairs at the Large Hadron Collider (LHC) are gluon-gluon (gg) fusion and quark-antiquark ($q\bar{q}$) annihilation, shown in Figure 1. The production cross section depends on the strong coupling constant α_s but is nearly independent on λ. The results of this study are based on the assumption that λ is sufficiently small that single-LQ production can be neglected.

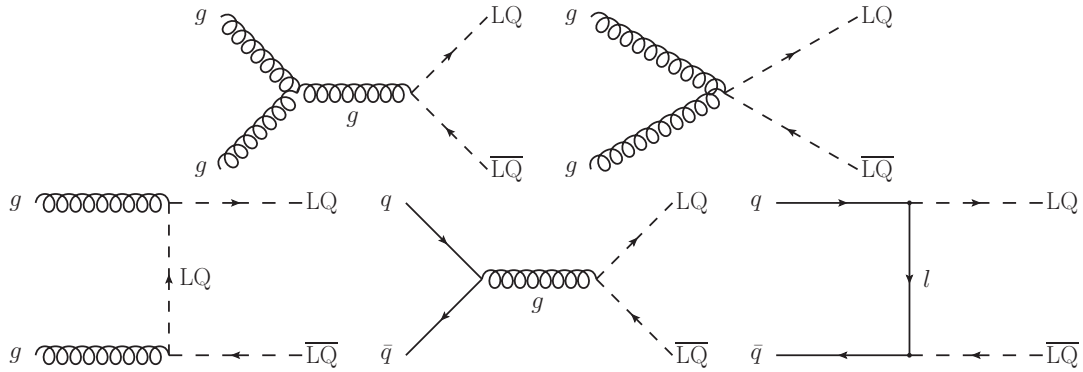

Figure 1: Dominant leading order diagrams for the pair production of scalar leptoquarks.

Several experiments have set limits on leptoquarks [11, 12] prior to this analysis. The most stringent limits on first generation leptoquarks prior to this search come from CMS, which excluded first generation leptoquarks with mass less than 830 (640) GeV for $\beta = 1(0.5)$ at 95% confidence level [13] using 5 fb^{-1} of data at $\sqrt{s} = 7$ TeV.

This paper presents the results of a search for pair-production of first generation scalar LQs. In this search, β is left as a free parameter, and two different channels are considered. The first channel ($eejj$) uses events containing two electrons and at least two jets and is most sensitive to scenario where $\beta = 1$. The second channel ($evjj$) uses events containing one electron, missing transverse energy ($E_{\mathrm{T}}^{\mathrm{miss}}$), and at least two jets. This search was conducted using proton-proton collision data at $\sqrt{s} = 8$ TeV. The data were collected in 2012 by the Compact Muon Solenoid (CMS) detector at the CERN Large Hadron Collider (LHC) and correspond to an integrated luminosity of 19.6 fb^{-1}.

2 The CMS detector

CMS uses a coordinate system with its origin at the nominal collision point. The x-axis points towards the center of the LHC. The y-axis points up towards the surface, perpendicular to the plane of the LHC. The z-axis points along the LHC beamline in the counter-clockwise direction. An azimuthal angle, ϕ, is defined with respect to the x-axis in the xy-plane, and a polar angle, θ, is defined with respect to the z-axis. Pseudorapidity, η, is defined as $\eta = -\ln(\tan(\theta/2))$.

A characteristic feature of the CMS detector is a superconducting solenoid. The solenoid is 6 m in diameter and produces a field of 3.8 T. A silicon inner tracker, an homogeneous electromagnetic calorimeter (ECAL) made of lead tungstate crystals, and a sampling hadronic calorimeter (HCAL) made of plastic scintillator and brass absorber are contained within the solenoid. A sampling hadronic calorimeter made of iron absorber and quart-fiber scintillators covers the forward region. Muons are detected using gas-ionization chambers located outside of the solenoid and embedded within a steel return yoke.

The inner tracker consists of a pixel detector and a silicon strip tracker, and it covers the pseudorapidity range $|\eta| < 2.5$. The resolutions on the transverse momentum (p_T) and impact parameter (d_0) of a charged particle with $p_T < 40$ GeV are typically 1% and 15 mm, respectively. The ECAL covers the pseudorapidity range $|\eta| < 3.0$, and provides an electron energy resolution of better than 0.5% for electrons with energies greater than 100 GeV. The HCAL covers the pseudorapidity range $|\eta| < 5.0$ and provides a jet energy resolution of about $100\%/\sqrt{E}$. The CMS detector is nearly hermetic, which allows for a momentum-balance measurement in the transverse plane (E_T^{miss}). A full description of the CMS detector is provided elsewhere [14].

3 Data and Simulation Samples

For the LQ searches in both the *eejj* channel and the *evjj* channel, events are selected using the unprescaled electron + dijet high level trigger (HLT) path, which requires at least one electron with $p_T > 30$ GeV, at least one jet with $p_T > 100$ GeV, and at least one other jet with $p_T > 25$ GeV. For the determination of the QCD multijet background in both the *eejj* channel and the *evjj* channel, events are selected using prescaled single photon triggers. These triggers require at least one ECAL deposit with varying p_T thresholds and identification requirements. For the determination of the $t\bar{t}$ background in the *eejj* channel only, which is determined using an *eμjj* sample, events are selected using an unprescaled single muon trigger. This trigger requires a muon with $p_T > 40$ GeV and $|\eta| < 2.1$; there are no isolation requirements.

Signal samples for leptoquark masses from 300 to 1200 GeV in both *eejj* ($LQ\overline{LQ} \to eqe\bar{q}$) and *evjj* ($LQ\overline{LQ} \to eq\nu\bar{q}'$) final states were generated with the PYTHIA event generator (version 6.422) and CTEQ6L1 parton distribution functions. All signal samples were generated with $\lambda = \lambda_{em} = 0.3$. Table 1 shows the leptoquark pair production NLO cross section and the relative theoretical uncertainties as a function of the leptoquark mass [15].

The dominant sources of *eejj* and *evjj* events from production of standard model particles are pair-production of top quarks and associated production of a Z^0 or W boson with jets. Smaller background contributions come from QCD multijet events, single top, diboson, and γ+jets production. Simulation samples are used to estimate or cross-check the contribution from all of these backgrounds. These samples are described below:

- W+jets, Z^0+jets, and $t\bar{t}$ events were generated using MADGRAPH [16].
- γ+jets and diboson (WW, WZ, ZZ) events were generated using PYTHIA [17].

Table 1: Details of the simulation signal datasets used in the analysis. Table includes NLO cross sections [pb], PDF uncertainty, and NLO cross-sections with the renormalization/factorization scale varied between half and twice the leptoquark mass [15].

M_{LQ} [GeV]	$\sigma(\mu = M_{\mathrm{LQ}})$ [pb]	$\delta(PDF)$ [pb]	$\sigma(\mu = M_{\mathrm{LQ}}/2)$ [pb]	$\sigma(\mu = M_{\mathrm{LQ}} \times 2)$ [pb]
300	1.89	0.214	1.63	2.13
350	0.77	0.102	0.663	0.866
400	0.342	0.052	0.295	0.385
450	0.163	0.0278	0.14	0.183
500	0.082	0.0155	0.0704	0.0922
550	0.0431	0.00893	0.037	0.0485
600	0.0235	0.0053	0.0201	0.0265
650	0.0132	0.00322	0.0113	0.0149
700	0.00761	0.002	0.00648	0.00858
750	0.00448	0.00126	0.00381	0.00506
800	0.00269	0.00081	0.00228	0.00304
850	0.00164	0.000527	0.00139	0.00186
900	0.00101	0.000347	0.000856	0.00115
950	0.000634	0.000231	0.000534	0.000722
1000	0.000401	0.000155	0.000337	0.000458
1050	0.000256	0.000105	0.000214	0.000293
1100	0.000165	7.18e-05	0.000138	0.000189
1150	0.000107	4.92e-05	8.88e-05	0.000123
1200	6.96e-05	3.4e-05	5.77e-05	8.04e-05

- Single-top events were generated using POWHEG [18].

For the MADGRAPH and POWHEG samples, parton showering and hadronization were performed with PYTHIA. CTEQ6L [19] parton distribution functions (PDFs) were used for all of these samples. The presence of pileup events is included in the simulation, and a re-weighting of simulation events for pileup is applied to match with the number of pileup events observed in data.

4 Reconstruction of Electrons, Muons, Jets, and $E_{\mathrm{T}}^{\mathrm{miss}}$

Energy clusters in the ECAL are matched to hits in the silicon pixel detector. Those hits in the pixel detector are then used to seed tracks in the rest of the tracker. The resulting pairs of ECAL energy clusters and tracker tracks form electron candidates. These candidates are required to have transverse energy (E_{T}) > 35 GeV and pseudorapidity $|\eta| < 2.5$, excluding the transition region between the barrel and endcap detectors, $1.442 < |\eta| < 1.56$. The selection criteria for electron ID and isolation [20], which are optimized for electrons with energies of hundreds of GeV have been applied. Electrons passing this selection are referred to as tight electrons.

Muon candidates are reconstructed as tracks in the muon system that are matched to a track that has been reconstructed by the inner tracking system [21]. For this analysis, muons must have $p_{\mathrm{T}} > 10$ GeV and satisfy a set of tight muon identification requirements. These include the requirements that muons must be reconstructed as global muons with at least one muon chamber hit included in the global-muon track fit, and segments in at least two muon stations. In addition, the muons must be isolated: the isolation energy within a cone of $\Delta\mathrm{R} = \sqrt{(\Delta\phi)^2 + (\Delta\eta)^2} > 0.4$ from the muon divided by the muon's transverse energy must be less than 0.12. This isolation energy is calculated using particle-flow algorithms [22, 23] and is corrected for pileup contamination. Jets are reconstructed by the anti-k_T algorithm [24] from a list of particles obtained using particle-flow methods and a radius parameter $R = 0.5$. The particle-flow algorithm [22, 23] reconstructs a complete, unique list of particles in each event using an optimized combination of information from all CMS subdetector systems. In addition to calorimeter noise cleaning at reconstruction level, loose jet identification criteria are applied to further remove fake jets due to electronic noise or other detector artifacts. The jet energy scale is derived using simulation and *in situ* measurements using dijet and photon+jet events. Jets are required to have $p_{\mathrm{T}} > 45$ GeV and $|\eta| < 2.4$. Each jet is also required to be separated by $\Delta\mathrm{R} = \sqrt{(\Delta\phi)^2 + (\Delta\eta)^2} > 0.3$ from each selected electron or muon candidate.

The missing transverse energy, $E_{\mathrm{T}}^{\mathrm{miss}}$, of the event is computed as the negative vector sum of all particle flow objects' transverse momenta. Corrections are applied to the $E_{\mathrm{T}}^{\mathrm{miss}}$ to account for pileup, jet energy corrections, and a systematic shift of the $E_{\mathrm{T}}^{\mathrm{miss}}$ observed in the $x - y$ plane. More information about $E_{\mathrm{T}}^{\mathrm{miss}}$ performance during this running period can be found in Ref [25].

5 Event Selection

5.1 Event Selection in the *eejj* Channel

The two leading (in p_{T}) electrons and the two leading (in p_{T}) jets are used in the *eejj* analysis. The electrons and jets must pass the identification requirements described in Section 4. In addition, all events in the *eejj* analysis must pass the following kinematic cuts:

- the event must have triggered the electron + dijet HLT path described in Section 3;
- there must be exactly two electrons with $p_{\mathrm{T}} > 45$ GeV and $|\eta| < 2.5$;

- there must be at least 1 jet with $p_T > 125$ GeV and $|\eta| < 2.4$;
- there must be at least 2 jets with $p_T > 45$ GeV and $|\eta| < 2.4$;
- m_{ee}, the invariant mass of the two electrons, must be greater than 50 GeV;
- S_T, the scalar sum of the p_T of the two electrons and the two leading jets, must be greater than 300 GeV;
- there must be no muons passing the tight identification requirements and having $p_T > 10$ GeV in the event.

The above selection is referred to as the $eejj$ preselection.

After applying the $eejj$ preselection, signal-to-background separation is optimized for each leptoquark mass listed in Table 1 by selecting values for cuts on the following variables that maximize $S/\sqrt{S+B}$, where S (B) represents the number of signal (background) events passing a given selection:

- m_{ee};
- S_T;
- $m_{ej}^{average}$ (m_{ej}^{min}), the average (minimum) electron-jet invariant mass of the two leptoquark candidates, obtained from the two electrons and two jets. There are two possible ways to combine two electrons and two jets to form two leptoquark candidates. The combination with the smaller difference between the two electron-jet masses is considered in this analysis. For the chosen combination, the value of $m_{ej}^{average}$ is the average between the two masses.

The optimized minimum cut values for each leptoquark mass are given in Table 2. Due to predicted backgrounds of less than one event, the cut values for leptoquarks with mass greater than or equal to 1000 GeV are all the same.

Table 2: Optimized final selection minimum criteria for the $eejj$ analysis for different LQ mass hypotheses.

	LQ mass ($eejj$)														
	300	350	400	450	500	550	600	650	700	750	800	850	900	950	≥ 1000
S_T [GeV]	435	485	535	595	650	715	780	850	920	1000	1075	1160	1245	1330	1425
m_{ee} [GeV]	110	110	115	125	130	140	145	155	160	170	175	180	190	195	205
m_{ej}^{min} [GeV]	50	105	160	205	250	290	325	360	390	415	435	450	465	470	475

5.2 Event Selection in the $evjj$ Channel

The leading (in p_T) electron, the two leading (in p_T) jets, and the E_T^{miss} are used in the $evjj$ analysis. The electrons and jets must pass the identification requirements described in Section 4. In addition, all events in the $evjj$ analysis must pass the following kinematic cuts:

- the event must have triggered the electron + dijet HLT path described in Section 3;
- there must be exactly one electron with $p_T > 45$ GeV and $|\eta| < 2.1$;
- there must be at least 1 jet with $p_T > 125$ GeV and $|\eta| < 2.4$;
- there must be at least 2 jets with $p_T > 45$ GeV and $|\eta| < 2.4$;
- E_T^{miss}, the missing transverse energy in the event, must be greater than 55 GeV;
- $\Delta\phi(E_T^{miss}, e)$, the azimuthal separation between the E_T^{miss} and the electron must be greater than 0.8;

- $\Delta\phi(E_{\mathrm{T}}^{\mathrm{miss}}, \mathrm{j1})$, the azimuthal separation between the $E_{\mathrm{T}}^{\mathrm{miss}}$ and the leading jet must be greater than 0.5;
- $\min\Delta R(\mathrm{e}, \mathrm{jets})$, the total angular separation between the electron and either of the jets must be greater than 0.7;
- S_{T}, the scalar sum of the p_{T} of the electron, the $E_{\mathrm{T}}^{\mathrm{miss}}$, and the two leading jets, must be greater than 300 GeV;
- there must be no muons passing the tight identification requirements and having $p_{\mathrm{T}} > 10$ GeV in the event.

The above selection is referred to as the $e\nu jj$ preselection.

After applying the $e\nu jj$ preselection, signal-to-background separation is optimized for each leptoquark mass listed in Table 1 by selecting values for cuts on the following variables that maximize $S/\sqrt{S+B}$:

- $E_{\mathrm{T}}^{\mathrm{miss}}$;
- S_{T};
- $m_{\mathrm{T,\,e\nu}} = \sqrt{2 \cdot p_{\mathrm{T,e}} \cdot E_{\mathrm{T}}^{\mathrm{miss}} (1 - \cos(\Delta\phi(E_{\mathrm{T}}^{\mathrm{miss}}, e)))}$, the electron-neutrino transverse mass;
- m_{ej} and $m_{\mathrm{T},\nu j}$, the electron-jet invariant mass and the neutrino-jet transverse mass of the two leptoquark candidates, obtained from the electron, the $E_{\mathrm{T}}^{\mathrm{miss}}$, and the two leading jets. There are two possible ways to combine one electron, one neutrino (i.e. $E_{\mathrm{T}}^{\mathrm{miss}}$) and two jets to form two leptoquark candidates. The combination with the smaller difference between the electron-jet transverse mass and the neutrino-jet transverse mass is considered in this analysis.

The optimized cut values for each leptoquark mass are given in Table 3. Due to predicted backgrounds of less than one event, the cut values for leptoquarks with mass greater than or equal to 950 GeV are all the same.

Table 3: Optimized final selection criteria for the $e\nu jj$ analysis for different LQ mass hypotheses

	LQ Mass ($e\nu jj$)													
	300	350	400	450	500	550	600	650	700	750	800	850	900	≥ 950
S_{T} [GeV]	495	570	645	720	800	880	960	1040	1120	1205	1290	1375	1460	1545
$E_{\mathrm{T}}^{\mathrm{miss}}$ [GeV]	90	95	100	110	115	125	135	145	155	170	180	195	210	220
m_{ej} [GeV]	195	250	300	355	405	455	505	555	600	645	695	740	780	825
$m_{\mathrm{T,\,e\nu}}$ [GeV]	125	150	175	200	220	240	255	270	280	290	295	300	300	300

6 Background estimates

6.1 Background estimate in the $eejj$ analysis

The Standard Model backgrounds contributing to the $eejj$ analysis are Z^0+jets (which dominates), $\mathrm{t\bar{t}}$, QCD multijets, diboson (WW, WZ, ZZ) production, single top production, $\mathrm{W}^{\pm}$+jets, and γ+jets. The methods used to estimate the contributions from the first three backgrounds are described below. The contribution from the remaining backgrounds is small at final selection, and it is estimated with simulation.

The contribution from the leading background (Z^0+jets) is determined using simulation that has been normalized to data within a control region. The Z^0+jets simulation is rescaled at

eejj preselection within a Z^0+jets-enriched region with $70 < m_{ee} < 110$, using Equation 1:

$$\mathcal{R}_{Z^0} = \frac{N_{data} - (N_{Others} + N_{QCD})}{N_{Z^0}} = 0.97 \pm 0.01 \text{ (stat)} \quad (1)$$

where N_{data}, N_Z, N_{Others}, N_{QCD} are, respectively, the number of events observed data in the Z^0+jets-enriched region, the number of events predicted from Z^0+jets simulation in the region, the number of events predicted from the simulation of other Standard Model backgrounds in the region, and QCD multijet events in the region. After this rescaling, good agreement is observed between the Standard Model background prediction and the observed events in data, both in terms of event yield and in terms of the shapes of the final selection variable distributions.

The contribution from the second leading background ($t\bar{t}$) is determined from data, using a $t\bar{t}$-enriched sample with exactly one tight electron, exactly one muon passing a set of tight muon identification requirements, and at least two jets. This sample is referred to as the *eμjj* sample. Events in the *eμjj* sample are selected online using an unprescaled trigger that requires a single muon with no isolation requirement. Each event in the *eμjj* sample is weighted to account for the different reconstruction efficiencies between electrons and muons and to account for the different number of *ee* and *eμ* events coming from $t\bar{t}$ production. The reweighted *eμjj* sample predicts 1579.6 ± 29.3 $t\bar{t}$ events will pass the *eejj* final selection, while the $t\bar{t}$ simulation predicts 1582.2 ± 13.8 $t\bar{t}$ events (uncertainties are statistical only). In addition, good agreement is observed between the reweighted *eμjj* sample and the *eejj* $t\bar{t}$ simulation in modeling the shape S_T and m_{ej} distributions at *eejj* preselection. These distributions are shown in Figure 2.

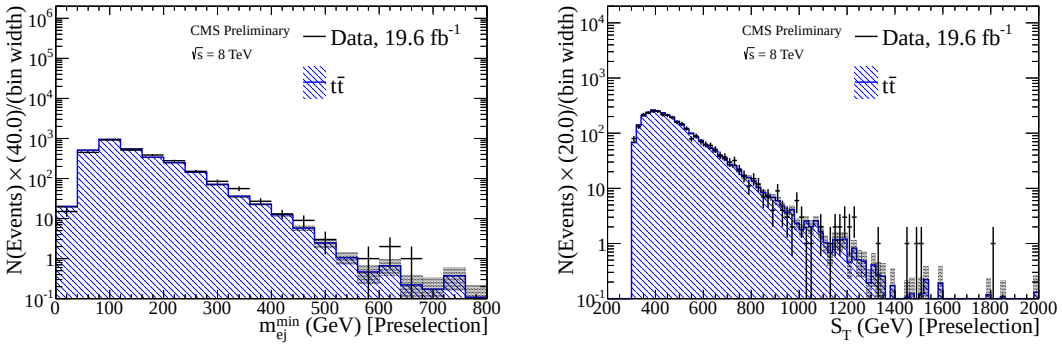

Figure 2: Comparison between events from data in the reweighted *eμjj* control sample and events from $t\bar{t}$ simulation at *eejj* preselection. The reweighted *eμjj* control sample accurately models the shape of the m_{ej}^{min} distribution (left) and the S_T distribution (right) of events coming from $t\bar{t}$ at the *eejj* preselection. The grey bands represent the statistical uncertainty on the background prediction only.

The QCD multijet background is determined from data using a 'fake rate' method. In this method, the probability of a jet being reconstructed as an electron that passes the electron selection is measured. The measurement is performed using a dataset collected with a prescaled single photon trigger, as described in Section 3. To suppress events with real $Z \to ee$ events, events are selected with only one reconstructed electron passing a loose ID and having $p_T > 10$ GeV and two or more jets with $p_T > 45$ GeV. This dataset is dominated by multijet events containing jets that have been misreconstructed as electrons. Other processes are subtracted using simulation. The fake rate (FR) is defined as the number of events in the dataset for which the electron passes the tight electron requirements over the total number of events in the sample.

This fake rate is measured as a function of electron p_{T}, and the result is binned in three electron η regions ($|\eta| < 1.442$, $1.56 < |\eta| < 2.00$, and $2.00 < |\eta| < 2.50$).

The QCD multijet background is estimated from a sample of events containing exactly two electrons passing a loose ID and at least two jets. Events in which either of the loose electrons pass the tight electron ID are removed from this sample, in order to protect against signal contamination. The QCD multijet background is estimated by weighting each of the events in this sample by $FR/(1-FR)$ for each electron. A consistency check performed on data suggests a systematic uncertainty of 60% in the *eejj* analysis. This estimate for the QCD multijet contribution is used in all plots, tables, and limits for the *eejj* analysis.

6.2 Background estimate in the *evjj* analysis

The Standard Model backgrounds contributing to the *evjj* analysis are $\mathrm{t\bar{t}}$ (which dominates), $\mathrm{W}^{\pm}$+jets, QCD multijets, diboson (WW, WZ, ZZ) production, single top production, Z^0+jets, and γ+jets. The methods used to estimate the contributions from the first three backgrounds are described below. The contribution from the remaining backgrounds is small at final selection, and it is estimated with simulation.

The contributions from the leading backgrounds ($\mathrm{W}^{\pm}$+jets and $\mathrm{t\bar{t}}$) are determined using simulation that has been normalized to data within control regions. Two separate control regions are used: one that enriches the samples with the $\mathrm{t\bar{t}}$ events and one that enriches the samples with the W+jets events. The $\mathrm{t\bar{t}}$-enriched sample (Sample 1) includes events that pass the *evjj* preselection, have $70 < m_{\mathrm{T,\,e\nu}} < 110$ GeV, and have four or more jets. The $\mathrm{W}^{\pm}$+jets-enriched sample (Sample 2) includes events that pass the *evjj* preselection, have $70 < m_{\mathrm{T,\,e\nu}} < 110$ GeV, and have fewer than four jets. These samples are used to define a system of equations:

$$\begin{cases} N^1_{\mathrm{data}} = \mathcal{R}_{\mathrm{t\bar{t}}} N^1_{\mathrm{t\bar{t}}} + \mathcal{R}_W N^1_W + N^1_{\mathrm{QCD}} + N^1_{\mathrm{Others}} \\ N^2_{\mathrm{data}} = \mathcal{R}_{\mathrm{t\bar{t}}} N^2_{\mathrm{t\bar{t}}} + \mathcal{R}_W N^2_W + N^2_{\mathrm{QCD}} + N^2_{\mathrm{Others}} \end{cases} \tag{2}$$

where $N^{\mathrm{i}}_{\mathrm{data}}$, N^{i}_W, $N^{\mathrm{i}}_{\mathrm{Others}}$, $N^{\mathrm{i}}_{\mathrm{t\bar{t}}}$, and $N^{\mathrm{i}}_{\mathrm{QCD}}$ are, respectively, the number of events in data, W+jets simulation (before rescaling), other simulated backgrounds (single-top, diboson, etc.), $\mathrm{t\bar{t}}$ simulation (before rescaling), and QCD multijet events passing selection i. Solving the system yields the following rescaling factors for the MADGRAPH $\mathrm{t\bar{t}}$ and W+jets samples:

$$\begin{aligned} \mathcal{R}_{\mathrm{t\bar{t}}} &= 0.97 \pm 0.02\ (\mathrm{stat}) \pm 0.01\ (\mathrm{syst}) \\ \mathcal{R}_{\mathrm{W}} &= 0.85 \pm 0.01\ (\mathrm{stat}) \pm 0.01\ (\mathrm{syst}) \end{aligned} \tag{3}$$

The value of $\mathcal{R}_{\mathrm{W}} = 0.85 \pm 0.01\ (\mathrm{stat}) \pm 0.01\ (\mathrm{syst})$ is determined primarily by the efficiency with which the trigger selects $\mathrm{W}^{\pm}$+jets events. After this rescaling, good agreement is observed between the Standard Model background prediction and the observed events in data, both in terms of event yield and in terms of the shapes of the final selection variable distributions.

The QCD multijet background is determined from data using a 'fake rate' method. The same electron fake rate measurement described in Section 6.1 for the *eejj* analysis is used in the *evjj* analysis. The QCD multijet background is estimated from a sample of events containing exactly one electron passing a loose ID, at least two jets, and large $E^{\mathrm{miss}}_{\mathrm{T}}$. Events in which the loose electron passes the tight electron ID are removed from this sample, in order to protect against signal contamination. The QCD multijet background is estimated by weighting each of the events in this sample by $FR/(1-FR)$. A consistency check performed on data suggests a systematic uncertainty of 30% in the *evjj* analysis. This estimate for the QCD multijet contribution is used in all plots, tables, and limits for the *evjj* analysis.

7 Comparison with data

7.1 Comparison with data in the *eejj* channel

Good agreement is observed when comparing data to background estimates at preselection level in the *eejj* analysis, as shown in Figure 3. Data and background estimates at the final selections optimized for a leptoquark with a mass of 450 GeV and a mass of 650 GeV are shown in Figures 4 and 5, respectively. Numerical comparisons between the number of background events and signal events predicted and number of events observed in data are shown in Table 4.

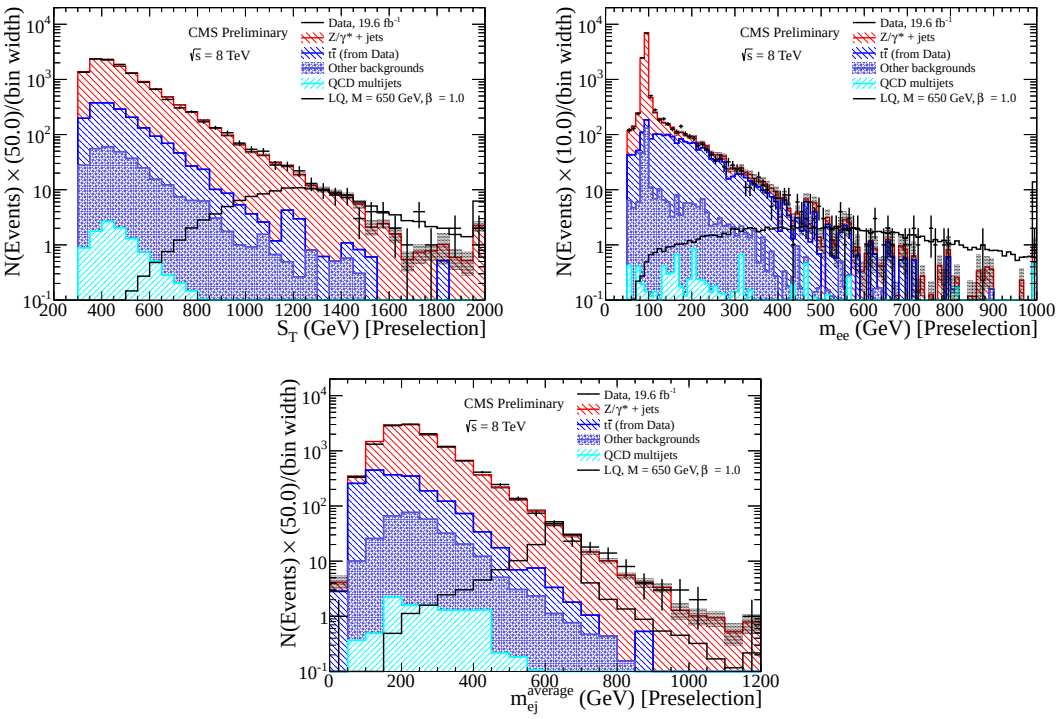

Figure 3: The S_{T} (top-left), m_{ee} (top-right), and $m_{\mathrm{ej}}^{\mathrm{average}}$ (bottom) distributions for events passing the *eejj* preselection. The grey bands represent the statistical uncertainty on the background prediction only.

In the final selection plots in Figures 4 and 5 and in Table 4, a broad excess is clearly visible for all selections optimized for a leptoquark of mass greater than 300 GeV. This excess is most significant in the selection optimized for a leptoquark of mass 650 GeV, where 20.49 ± 2.14 (stat) ± 2.45 (syst) events are expected and 36 events are observed. The significance of the observed data with respect to the background estimate at this selection is 2.4. Unlike predicted leptoquark signal, the excess does not peak sharply in the $m_{\mathrm{ej}}^{\mathrm{min}}$ distribution.

7.2 Comparison with data in the *evjj* channel

Good agreement is observed when comparing data to background estimates at preselection level in the *evjj* analysis, as shown in Figure 6. Data and background estimates at the final selections optimized for a leptoquark with a mass of 450 GeV and a mass of 650 GeV are shown in Figures 7 and 8, respectively. Numerical comparisons between the number of background events and signal events predicted and number of events observed in data are shown in Table 5.

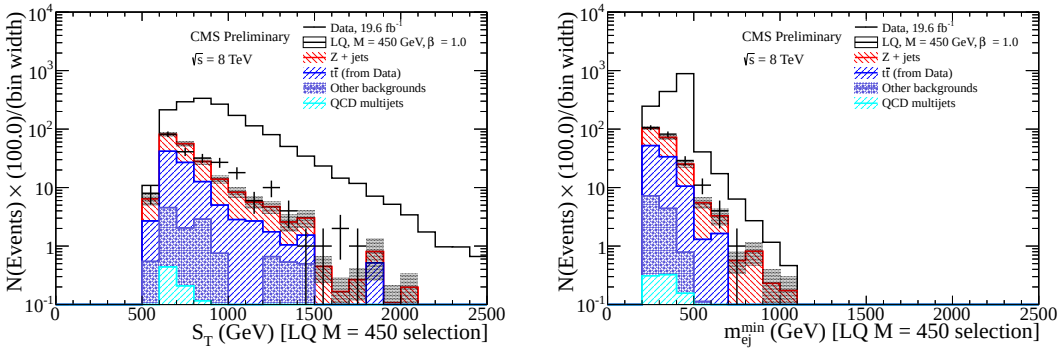

Figure 4: The S_{T} (left) and $m_{\mathrm{ej}}^{\mathrm{min}}$ (right) distributions for events passing the full *eejj* selection optimized for $M_{\mathrm{LQ}} = 450$ GeV. The grey bands represent the statistical and systematic uncertainty on the background prediction.

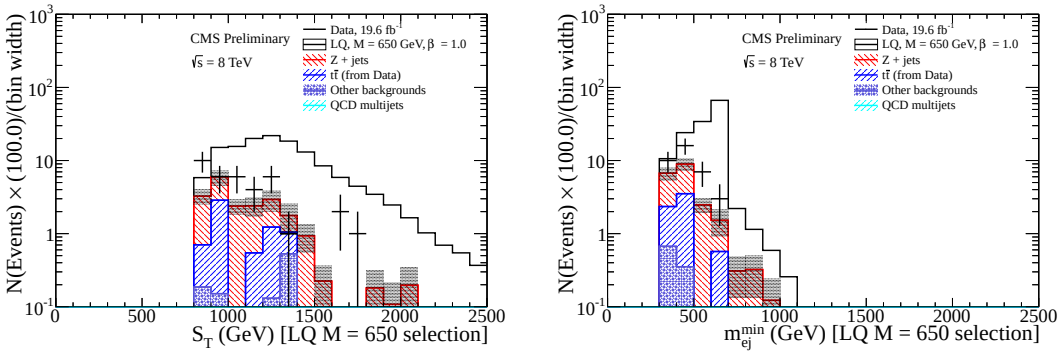

Figure 5: The S_{T} (left) and $m_{\mathrm{ej}}^{\mathrm{min}}$ (right) distributions for events passing the full *eejj* selection optimized for $M_{\mathrm{LQ}} = 650$ GeV. The grey bands represent the statistical and systematic uncertainty on the background prediction.

Table 4: Number of events after final *eejj* selection. Only statistical errors are reported, except in the "Total Background" column, where systematic uncertainties are also reported. The "Significance" column provides the significance of the excess observed in data with respect to the background prediction after accounting for the correlations of the systematic uncertainties; no signal hypothesis is included in the calculation.

M_{LQ}	LQ Signal	Z+Jets	$t\bar{t}$ (from data)	QCD (from data)	Other	Data	Total Background	Significance
Presel	-	10538.4 ± 35.8	1566.6 ± 29.2	10.87 ± 0.10	303.8 ± 7.4	12442	12419.6 ± 46.8	NA
300	13560.2 ± 80.1	462.2 ± 7.4	724.3 ± 19.8	5.282 ± 0.052	62.1 ± 4.6	1244	$1253.94 \pm 21.67 \pm 30.08$ (syst)	0.0
350	6473.9 ± 33.3	332.1 ± 6.2	352.0 ± 13.8	3.215 ± 0.036	37.7 ± 3.6	736	$725.10 \pm 15.57 \pm 24.99$ (syst)	0.0
400	3089.3 ± 15.0	203.2 ± 4.8	153.7 ± 9.1	1.696 ± 0.023	23.8 ± 2.9	389	$382.40 \pm 10.72 \pm 15.00$ (syst)	0.0
450	1508.1 ± 7.2	112.9 ± 3.5	86.9 ± 6.9	0.890 ± 0.016	11.8 ± 2.0	233	$212.44 \pm 7.99 \pm 13.33$ (syst)	0.0
500	767.4 ± 3.6	66.5 ± 2.7	47.2 ± 5.1	0.485 ± 0.011	7.4 ± 1.6	148	$121.61 \pm 5.96 \pm 6.03$ (syst)	1.8
550	410.5 ± 1.9	37.4 ± 2.1	25.8 ± 3.7	0.2758 ± 0.0084	3.7 ± 1.1	81	$67.24 \pm 4.40 \pm 3.39$ (syst)	0.7
600	225.7 ± 1.0	22.2 ± 1.6	14.2 ± 2.8	0.1527 ± 0.0065	3.12 ± 1.00	57	$39.66 \pm 3.35 \pm 2.42$ (syst)	2.1
650	125.85 ± 0.58	14.0 ± 1.2	5.4 ± 1.7	0.0760 ± 0.0040	1.05 ± 0.47	36	$20.49 \pm 2.14 \pm 2.45$ (syst)	2.4
700	72.88 ± 0.33	8.16 ± 0.93	4.3 ± 1.5	0.0448 ± 0.0029	0.21 ± 0.12	17	$12.74 \pm 1.80 \pm 2.15$ (syst)	0.9
750	43.10 ± 0.20	4.88 ± 0.69	1.55 ± 0.90	0.0258 ± 0.0023	0.078 ± 0.038	12	$6.53 \pm 1.13 \pm 1.09$ (syst)	1.6
800	26.17 ± 0.12	2.93 ± 0.52	1.04 ± 0.73	0.0193 ± 0.0022	0.078 ± 0.038	7	$4.06 \pm 0.90 \pm 0.89$ (syst)	1.1
850	15.978 ± 0.072	2.34 ± 0.48	0.52 ± 0.52	0.0111 ± 0.0015	0.042 ± 0.028	5	$2.91 \pm 0.71 \pm 0.71$ (syst)	0.0
900	9.813 ± 0.044	1.23 ± 0.36	0.52 ± 0.52	0.0069 ± 0.0012	0.022 ± 0.020	3	$1.77 \pm 0.63 \pm 0.37$ (syst)	0.0
950	6.086 ± 0.028	0.89 ± 0.29	$0.00^{+1.14}_{-0.00}$	0.00451 ± 0.00085	0.022 ± 0.020	1	$0.912^{+1.178}_{-0.295} \pm 0.27$ (syst)	0.0
1000	3.860 ± 0.018	0.56 ± 0.22	$0.00^{+1.14}_{-0.00}$	0.00374 ± 0.00082	0.0025 ± 0.0025	1	$0.567^{+1.162}_{-0.223} \pm 0.17$ (syst)	0.0
1050	2.576 ± 0.011	0.56 ± 0.22	$0.00^{+1.14}_{-0.00}$	0.00374 ± 0.00082	0.0025 ± 0.0025	1	$0.567^{+1.162}_{-0.223} \pm 0.17$ (syst)	0.0
1100	1.6936 ± 0.0072	0.56 ± 0.22	$0.00^{+1.14}_{-0.00}$	0.00374 ± 0.00082	0.0025 ± 0.0025	1	$0.567^{+1.162}_{-0.223} \pm 0.17$ (syst)	0.0
1150	1.1272 ± 0.0047	0.56 ± 0.22	$0.00^{+1.14}_{-0.00}$	0.00374 ± 0.00082	0.0025 ± 0.0025	1	$0.567^{+1.162}_{-0.223} \pm 0.17$ (syst)	0.0
1200	0.7498 ± 0.0030	0.56 ± 0.22	$0.00^{+1.14}_{-0.00}$	0.00374 ± 0.00082	0.0025 ± 0.0025	1	$0.567^{+1.162}_{-0.223} \pm 0.17$ (syst)	0.0

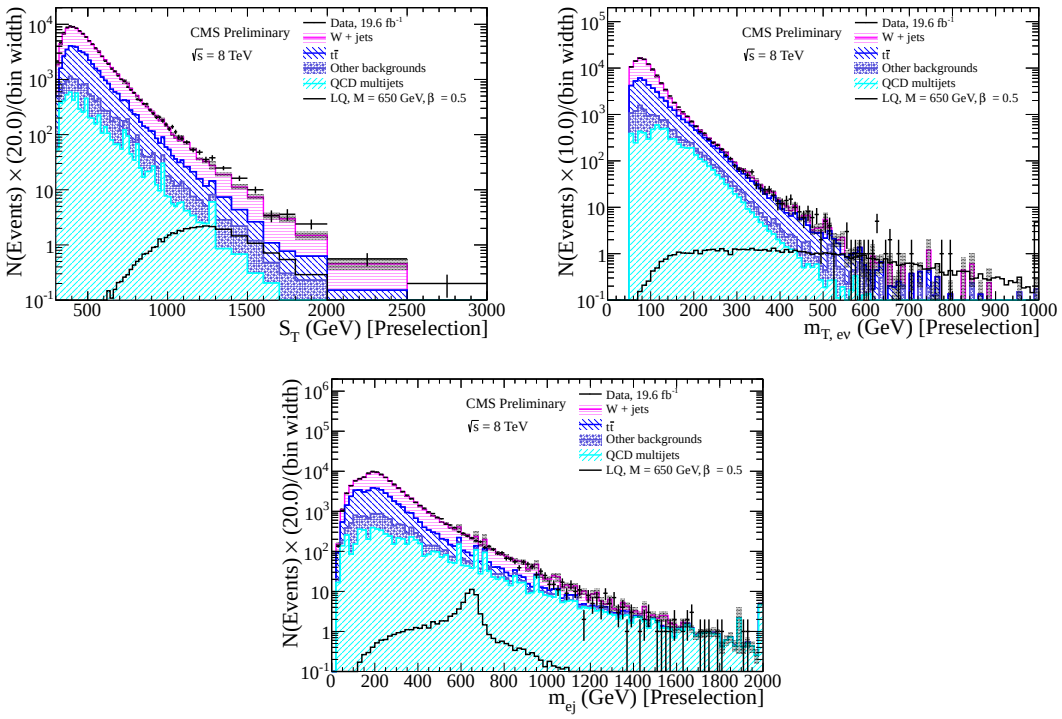

Figure 6: The S_{T} (top-left), $m_{\mathrm{T,\,e\nu}}$ (top-right), and m_{ej} distributions for events passing the *evjj* preselection. The grey bands represent the statistical uncertainty on the background prediction only.

In the final selection plots in Figures 7 and 8 and in Table 5, a broad excess is clearly visible for all final selections optimized for a leptoquark of mass greater than 300 GeV. As in the case of the *eejj* channel, this excess is most significant in the selection optimized for a leptoquark of mass 650 GeV, where 7.54 ± 1.20 (stat) ± 1.07 (syst) events are expected and 18 events are observed. The significance of the observed data with respect to the background estimate at this selection is 2.6. Unlike predicted leptoquark signal, the excess does not peak sharply in the m_{ej} distribution.

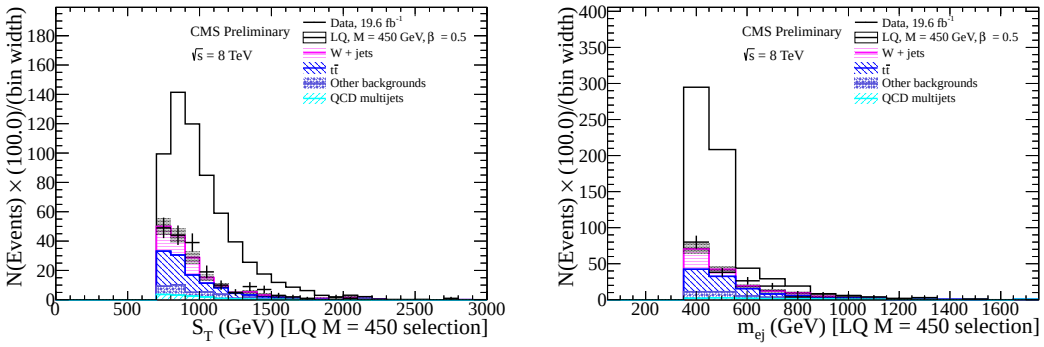

Figure 7: The S_{T} (left) and m_{ej} (right) distributions for events passing the full *evjj* selection optimized for $M_{\mathrm{LQ}} = 450$ GeV. The grey bands represent the statistical and systematic uncertainty on the background prediction.

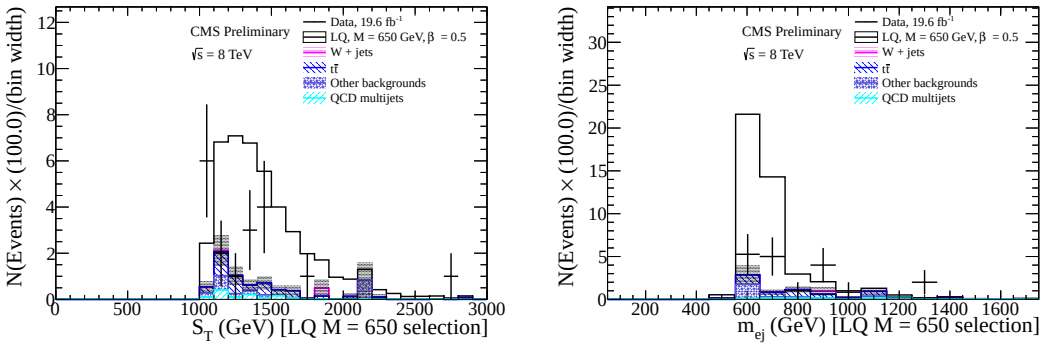

Figure 8: The S_{T} (left) and m_{ej} (right) distributions for events passing the full *evjj* selection optimized for $M_{\mathrm{LQ}} = 650$ GeV. The grey bands represent the statistical and systematic uncertainty on the background prediction.

8 Systematic uncertainties

The systematic uncertainties applied to this analysis are as follows:

- A 2.6% uncertainty on the integrated luminosity [26];
- A jet energy scale uncertainty depending on jet p_{T} and η [27];
- A jet energy resolution uncertainty depending on jet η [27];
- An electron energy scale uncertainty of 0.4% (4.1%) for electrons in the ECAL barrel (endcap) [20];
- An electron energy resolution uncertainty of 0.6% (1.5%) for electrons in the ECAL barrel (endcap) [28];

Table 5: Number of events after final *evjj* selection. Only statistical errors are reported, except in the "Total Background" column, where systematic uncertainties are also reported. The "Significance" column provides the significance of the excess observed in data with respect to the background prediction after accounting for the correlations of the systematic uncertainties; no signal hypothesis is included in the calculation.

M_{LQ}	LQ Signal	W+Jets	$t\bar{t}$	QCD	Other	Data	Total Background	Significance
Presel	-	58284.8 ± 197.0	32196.7 ± 69.8	5950.5 ± 20.1	6590.8 ± 231.6	105164	103022.8 ± 312.6	NA
300	4765.5 ± 51.1	822.1 ± 22.4	1191.3 ± 12.0	117.9 ± 1.5	210.5 ± 7.7	2455	$2341.90 \pm 26.58 \pm 329.79$ (syst)	0.3
350	2168.4 ± 21.6	275.9 ± 14.5	441.4 ± 7.2	59.11 ± 0.97	102.1 ± 5.4	908	$878.55 \pm 17.08 \pm 122.13$ (syst)	0.2
400	971.1 ± 9.6	110.4 ± 7.8	184.2 ± 4.7	32.88 ± 0.69	51.5 ± 3.8	413	$378.98 \pm 9.91 \pm 51.38$ (syst)	0.5
450	469.7 ± 4.6	53.1 ± 5.8	74.7 ± 3.0	14.13 ± 0.42	25.7 ± 2.7	192	$167.64 \pm 7.06 \pm 21.33$ (syst)	0.8
500	232.7 ± 2.3	20.5 ± 3.3	34.4 ± 2.0	7.76 ± 0.30	15.3 ± 2.1	83	$77.99 \pm 4.41 \pm 9.77$ (syst)	0.0
550	121.4 ± 1.2	8.6 ± 1.8	14.9 ± 1.4	3.89 ± 0.21	7.8 ± 1.6	44	$35.24 \pm 2.76 \pm 4.31$ (syst)	1.0
600	66.37 ± 0.66	2.3 ± 1.0	7.08 ± 0.93	2.29 ± 0.17	4.6 ± 1.2	28	$16.27 \pm 1.84 \pm 2.03$ (syst)	2.1
650	37.22 ± 0.37	0.41 ± 0.29	3.82 ± 0.70	1.18 ± 0.12	2.13 ± 0.92	18	$7.54 \pm 1.20 \pm 1.07$ (syst)	2.6
700	21.74 ± 0.21	0.41 ± 0.29	2.61 ± 0.60	0.85 ± 0.10	0.58 ± 0.24	6	$4.45 \pm 0.71 \pm 0.74$ (syst)	0.0
750	12.90 ± 0.13	$0.00^{+0.94}_{-0.00}$	1.75 ± 0.47	0.514 ± 0.091	0.27 ± 0.15	4	$2.535^{+1.062}_{-0.504} \pm 0.49$ (syst)	0.0
800	7.610 ± 0.075	$0.00^{+0.94}_{-0.00}$	1.10 ± 0.37	0.317 ± 0.067	0.27 ± 0.15	3	$1.696^{+1.019}_{-0.404} \pm 0.31$ (syst)	0.0
850	4.713 ± 0.046	$0.00^{+0.94}_{-0.00}$	0.90 ± 0.34	0.117 ± 0.029	0.140 ± 0.087	2	$1.153^{+0.999}_{-0.353} \pm 0.24$ (syst)	0.0
900	2.929 ± 0.028	$0.00^{+0.94}_{-0.00}$	0.37 ± 0.21	0.076 ± 0.024	0.084 ± 0.069	1	$0.530^{+0.962}_{-0.226} \pm 0.10$ (syst)	0.0
950	1.839 ± 0.018	$0.00^{+0.94}_{-0.00}$	0.37 ± 0.21	0.069 ± 0.023	0.084 ± 0.069	1	$0.524^{+0.962}_{-0.226} \pm 0.10$ (syst)	0.0
1000	1.306 ± 0.012	$0.00^{+0.94}_{-0.00}$	0.37 ± 0.21	0.069 ± 0.023	0.084 ± 0.069	1	$0.524^{+0.962}_{-0.226} \pm 0.10$ (syst)	0.0
1050	0.9022 ± 0.0076	$0.00^{+0.94}_{-0.00}$	0.37 ± 0.21	0.069 ± 0.023	0.084 ± 0.069	1	$0.524^{+0.962}_{-0.226} \pm 0.10$ (syst)	0.0
1100	0.6225 ± 0.0050	$0.00^{+0.94}_{-0.00}$	0.37 ± 0.21	0.069 ± 0.023	0.084 ± 0.069	1	$0.524^{+0.962}_{-0.226} \pm 0.10$ (syst)	0.0
1150	0.4308 ± 0.0032	$0.00^{+0.94}_{-0.00}$	0.37 ± 0.21	0.069 ± 0.023	0.084 ± 0.069	1	$0.524^{+0.962}_{-0.226} \pm 0.10$ (syst)	0.0
1200	0.2971 ± 0.0022	$0.00^{+0.94}_{-0.00}$	0.37 ± 0.21	0.069 ± 0.023	0.084 ± 0.069	1	$0.524^{+0.962}_{-0.226} \pm 0.10$ (syst)	0.0

- An uncertainty on the pileup modeling of 6%;
- A 60% (30%) uncertainty on QCD multijet background in the *eejj* (*evjj*) channel ;
- A 2% uncertainty on the scale factor for $e\mu jj$ sample for $t\bar{t}$ background estimate in the *eejj* channel;
- A 1% uncertainty on the scale factor for Z^0+jets simulation sample in the *eejj* channel;
- A 2% uncertainty on the scale factor for W+jets simulation sample in the *evjj* channel;
- A 3% uncertainty on the scale factor for the $t\bar{t}$ simulation sample in the *evjj* channel;
- Uncertainties on the Z^0+jets, $W^{\pm}$+jets, and $t\bar{t}$ shapes, as determined using MADGRAPH simulation; samples for which the renormalization and factorization scales and matching thresholds have been varied by a factor of two;
- An uncertainty on the signal acceptance and background acceptance and cross-section due to PDF uncertainty: 3% (2%) for background (signal) in the *eejj* channel and 3-25% (3%) for background (signal) in the *evjj* channel.

The effects of these uncertainties on the analysis is determined by varying the relevant parameters by the above uncertainties. The analysis is then repeated in full to determine the change in event yields for both signal and background predictions.

9 Results

Once the final selections have been applied across all leptoquark mass hypotheses in both analyses, limits on leptoquark mass may be set by comparing the number of events observed to pass those final selections with the number of events predicted by the various background estimates. A log-normal probability function is used to integrate over the statistical uncertainties described in Section 8. Statistical uncertainties are described with Γ distributions using a width determined by the number of simulated events or the number of events observed in control re-

gions in data that pass final selection criteria. Limits are set using the asymptotic CLs modified frequentist approach [29, 30].

Figure 9 shows the 95% CL upper limits on $\sigma \times \beta^2$ ($\sigma \times 2\beta(1-\beta)$) as a function of leptoquark mass for scalar leptoquarks in the $eejj$ ($e\nu jj$) channel. The solid black line denotes the observed limit, the dashed black line denotes the central value of the predicted limit, and the green and yellow bands denote the systematic uncertainty within one and two standard deviations of the central value of the predicted limit, respectively. The theoretical cross sections are shown as a blue line. A lighter blue band around that line denotes the combined theoretical uncertainty coming from both the factorization and PDF uncertainties, as shown in Figure 1. Using Figure 9, 95% CL exclusion limits are placed on first generation scalar leptoquarks with masses less than 1005 (845) GeV, assuming $\beta = 1.0$ (0.5). This is to be compared with expected 95% CL exclusions of 1030 (890) GeV, assuming $\beta = 1.0$ (0.5).

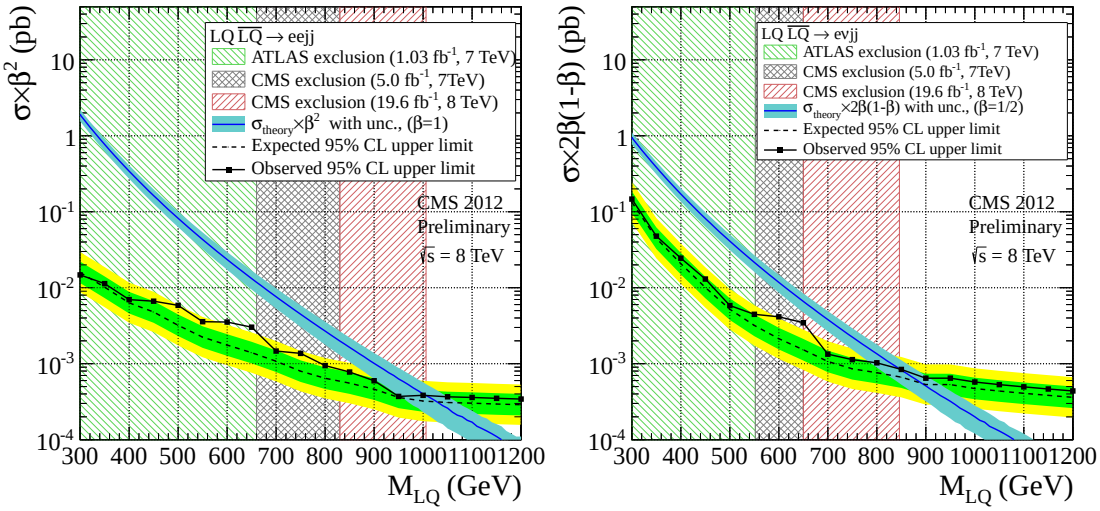

Figure 9: The expected and observed upper limit at 95% C.L. on the LQ pair production cross section times β^2 in the top plot ($2\beta(1-\beta)$ in the bottom plot) as a function of the LQ mass obtained with the $eejj$ ($e\nu jj$) analysis. /The systematic uncertainties described in the text are included in the calculation. The dark blue curve and the light blue band represent, respectively, the theoretical LQ pair production cross section and the uncertainties due to the choice of PDF and renormalization/factorization scales.

The two independent limits from the $eejj$ and $e\nu jj$ channels are combined in Figure 10. This combination results in a region of space in the β-mass plane which is excluded. The combination does not change the observed limits for the case where $\beta = 0.5$ or where $\beta = 1.0$ (Figure 9). These limits for $\beta = 0.5$ and $\beta = 1.0$ represent the most stringent limits on first generation leptoquarks to date.

Good agreement between observed events and the Standard Model background prediction is seen at preselection level for the S_T, m_{ee}, and m_{ej}^{min} distributions in the $eejj$ analysis (Figure 3) and for the S_T, $m_{T,e\nu}$, and m_{ej} distributions in the $e\nu jj$ analysis (Figure 6). In spite of this, Tables 4 and 5 and Figures 9 and 10 clearly show a broad excess of observed events in data in both channels with respect to the predicted contribution from Standard Model background in nearly all of the levels of final selection. The excess in both analyses is most significant for the final selection optimized for a leptoquark with a mass of 650 GeV. Figure 10 shows that a leptoquark of mass 650 GeV with $\beta < 0.15$ cannot be excluded by this analysis. This region of

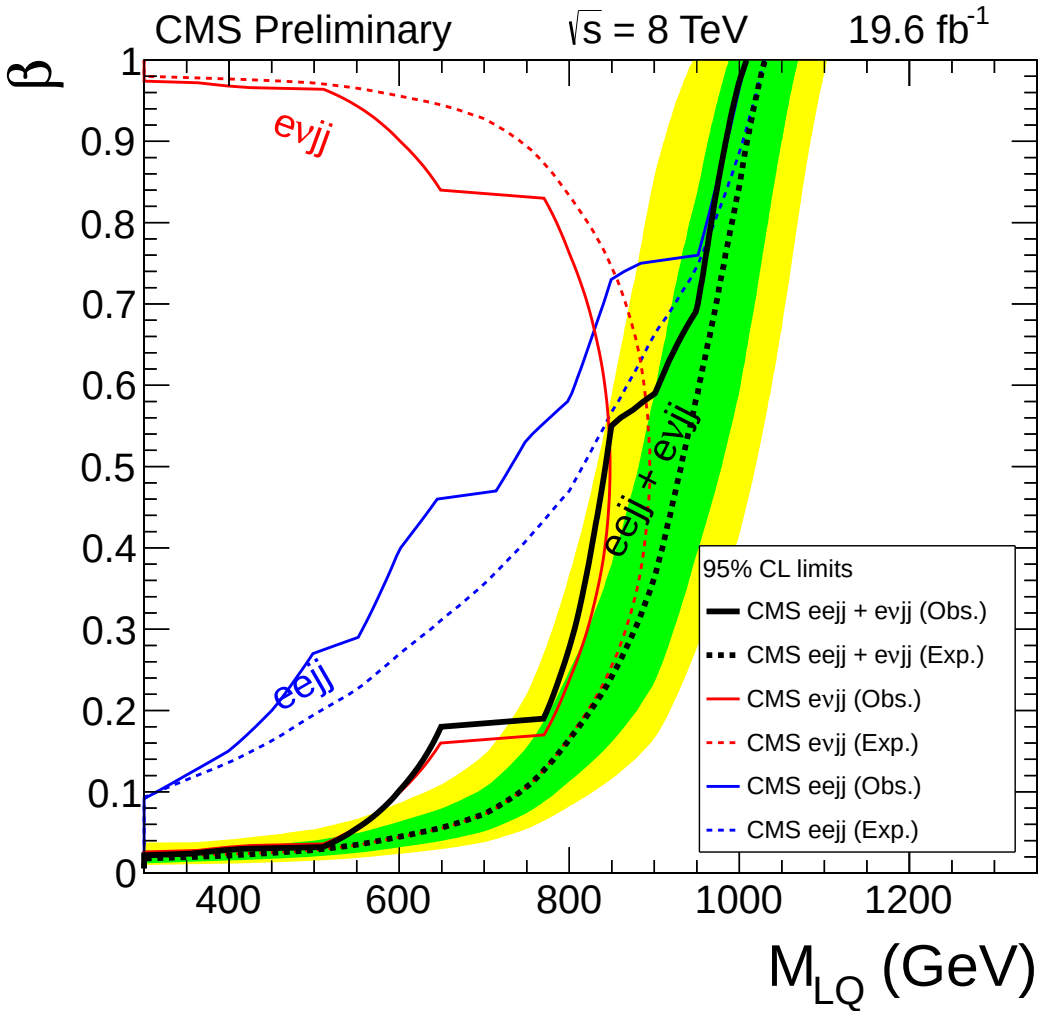

Figure 10: The expected and observed exclusion limits at 95% CL on the first generation leptoquark hypothesis in the β versus mass plane using the central value of signal cross section for the individual $eejj$ and $evjj$ channels and their combination. The green and yellow expected limit uncertainty bands represent the 68% and 95% confidence intervals. Solid lines represent the observed limits in each channel, and dashed lines represent the expected limits.

the parameter space is dominated by the $evjj$ analysis. The approximately 10 event excess in the $evjj$ final selection optimized for a leptoquark of mass 650 GeV corresponds to a leptoquark of mass 650 GeV and $\beta = 0.075$.

An investigation of the S_T and m_{ej}^{min} distributions in the $eejj$ analysis shows that the excess in that analysis is background-like. The excess events do not appear in tail of the S_T distribution, and the m_{ej}^{min} distribution does not peak sharply. A similar investigation in the $evjj$ analysis shows that the core of the S_T distribution is described well by the Standard Model background prediction, while the excess events appear in the distribution tail. Similarly, the m_{ej} distribution in the $evjj$ analysis is described well for low values of m_{ej}, where the Standard Model background dominates. The m_{ej}^{min} distribution in the $eejj$ analysis and the m_{ej} distribution in the $evjj$ analysis as compared the predicted contribution of Standard Model background and a leptoquark of mass 650 GeV and $\beta = 0.075$ are shown in Figure 11. In both analyses, the excess is not characterized by the presence of jets from bottom quarks, as identified by the combined secondary vertex b-tagging algorithm [31].

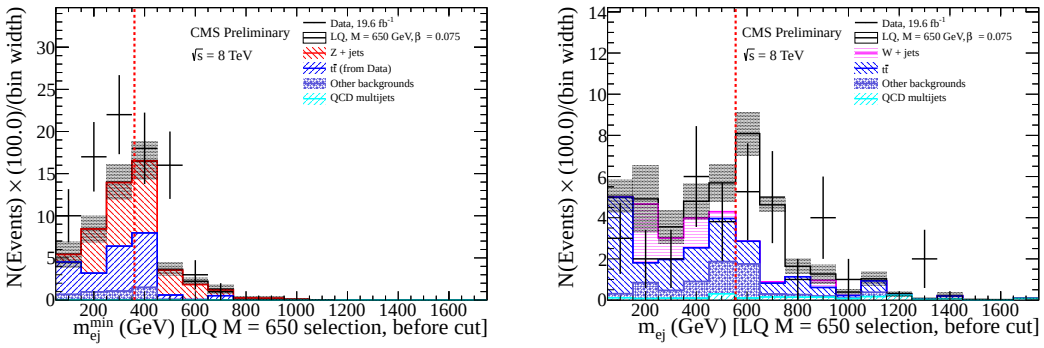

Figure 11: The m_{ej}^{min} distribution in the $eejj$ analysis (left) and the m_{ej} distribution in the $evjj$ analysis (right) after all other cuts defined for the final selection optimized for a leptoquark mass of 650 GeV have been applied. The red line corresponds to the value of the cut on m_{ej}^{min} (m_{ej}) in the $eejj$ ($evjj$) analysis. The signal in both distributions corresponds to a leptoquark with a mass of 650 GeV and $\beta = 0.075$. In the case of the $eejj$ analysis, less than one signal event with these parameters is expected to pass this selection. The grey bands correspond to the statistical and systematic errors on the Standard Model background and the statistical errors on the signal.

The excess in the $evjj$ channel is broader in the m_{ej} distribution than signal Monte Carlo prediction, but the limited number of observed events in data bar a more conclusive statement. The intrinsic width, Γ, of scalar leptoquarks is defined by the signal Monte Carlo to be $\Gamma = \frac{\lambda^2}{16\pi} \times M_{LQ}$, where λ corresponds to the coupling constant between leptoquark, lepton, and quark. The signal Monte Carlo used in this analysis corresponds to $\lambda = 0.3$, which corresponds to a width of roughly 13 GeV. Significantly higher values of λ (and consequently broader leptoquarks) are strongly limited in this mass range by results from the HERA experiments [32, 33]. This implies that the intrinsic width of leptoquarks of mass close to 650 GeV would be negligible compared to the experimental resolution.

Because the discrepancies in both channels are significantly less than what would be expected in the case of a leptoquark with a mass of 650 GeV and $\beta \geq 0.5$, 95% CL exclusion limits are placed on first generation scalar leptoquarks with masses less than 1005 (845) GeV, assuming $\beta = 1.0$ (0.5).

10 Conclusions

In summary, a search has been carried out for the pair production of first generation scalar leptoquarks decaying to two electrons and two jets or to one electron, one neutrino, and two jets. The data used in this search were collected in 2012 by the CMS detector and correspond to an integrated luminosity of 19.6 fb^{-1}. The selection criteria were optimized for each signal leptoquark mass hypothesis under consideration. In both channels, a significant excess is observed in the final selection optimized for leptoquarks with a mass of 650 GeV. The excess in the $evjj$ channel in particular makes it impossible to exclude leptoquarks with a mass of 650 GeV and $\beta < 0.15$. However, limits may still be placed with 95% CL on first generation scalar leptoquarks with masses less than 950 (845) GeV, assuming $\beta = 1.0(0.5)$. This is to be compared with expected 95% CL exclusions of 975 (890) GeV, assuming $\beta = 1.0(0.5)$. These limits for $\beta = 0.5$ and $\beta = 1.0$ represent the most stringent limits on first generation scalar leptoquarks to date.

References

[1] H. Georgi and S. Glashow, "Unity of All Elementary-Particle Forces", *Phys. Rev. Lett.* **32** (1974) 438, doi:10.1103/PhysRevLett.32.438.

[2] J. C. Pati and A. Salam, "Lepton Number as the Fourth Color", *Phys. Rev. D* **10** (1974) 275, doi:10.1103/PhysRevD.10.275.

[3] B. Schrempp and F. Schrempp, "Light Leptoquarks", *Phys. Lett.* **B153** (1985) 101, doi:10.1016/0370-2693(85)91450-9.

[4] S. Dimopoulos and L. Susskind, "Mass Without Scalars", *Nucl. Phys. B* **155** (1979) 237, doi:10.1016/0550-3213(81)90304-7.

[5] S. Dimopoulos, "Technicolored Signatures", *Nucl. Phys. B* **168** (1980) 69, doi:10.1016/0550-3213(80)90277-1.

[6] E. Eichten and K. Lane, "Dynamical Breaking of the Weak Interaction Symmetries", *Phys. Lett. B* **90** (1980) 85, doi:10.1016/0370-2693(80)90065-9.

[7] J. L. Hewett and T. G. Rizzo, "Low-energy Phenomenology of Superstring-inspired E_6 Models", *Phys. Lett.* **183** (1989) 193, doi:10.1016/0370-1573(89)90071-9.

[8] M. Kuze and Y. Sirois, "Search for particles and forces beyond the standard model in high energy lepton-hadron and hadron-hadron collisions", *Progress in Particle and Nuclear Physics* **50** (2003) 1, doi:10.1016/S0146-6410(02)00176-X.

[9] Particle Data Group Collaboration, "Review of Particle Physics", *Phys. Rev. D* **86** (2012) 010001, doi:10.1103/PhysRevD.86.010001.

[10] W. Buchmüller and D. Wyler, "Constraints on SU(5)-type Leptoquarks", *Phys. Lett. B* **177** (1986) 377, doi:10.1016/0370-2693(86)90771-9.

[11] ATLAS Collaboration, "Search for first generation scalar leptoquarks in pp collisions at with the ATLAS detector", *Phys. Lett. B* **709** (2012) 158, doi:10.1016/j.physletb.2012.02.004.

[12] ATLAS Collaboration, "Search for second generation scalar leptoquarks in pp collisions at $\sqrt{s} = 7$ TeV with the ATLAS detector", *Eur. Phys. C* **72** (2012) doi:10.1140/epjc/s10052-012-2151-6.

[13] CMS Collaboration, "Search for pair production of first- and second-generation scalar leptoquarks in pp collisions at $\sqrt{s} = 7$ TeV", *Phys. Rev. D* **86** (2012) 052013, doi:10.1103/PhysRevD.86.052013.

[14] CMS Collaboration, "The CMS experiment at the CERN LHC", *JINST* **3** (2008) S08004, doi:doi:10.1088/1748-0221/3/08/S08004.

[15] M. Krämer, T. Plehn, M. Spira, and P. M. Zerwas, "Pair production of scalar leptoquarks at the CERN LHC", *Phys. Rev. D* **71** (2005) 057503, doi:10.1103/PhysRevD.71.057503.

[16] J. Alwall et al., "MadGraph/MadEvent v4: the new web generation", *JHEP* **09** (2007) 028, doi:10.1088/1126-6708/2007/09/028.

[17] T. Sjstrand et al., "High-energy-physics event generation with Pythia6.1", *Comp. Phys. Comm.* **135** (2001) 238, doi:10.1016/S0010-4655(00)00236-8.

[18] S. Alioli, P. Nason, C. Oleari, and E. Re, "NLO vector-boson production matched with shower in POWHEG", *JHEP* **07** (2008) 060, doi:10.1088/1126-6708/2008/07/060.

[19] J. Pumplin et al., "New generation of parton distributions with uncertainties from global QCD analysis", *JHEP* **07** (2002) 012, doi:10.1088/1126-6708/2002/07/012.

[20] CMS Collaboration, "Search for Resonances in Dilepton Mass Spectra in pp Collisions at $\sqrt{s}$ = 8 TeV", *CMS Physics Analysis Summary: EXO-12-061* (2013).

[21] CMS Collaboration, "Performance of muon identification in pp collisions at $\sqrt{s}$ = 7 TeV", *CMS Physics Analysis Summary: MUO-10-002* (2010).

[22] CMS Collaboration, "Particle-Flow Event Reconstruction in CMS and Performance for Jets, Taus, and MET", *CMS Physics Analysis Summary: PFT-09-001* (2009).

[23] CMS Collaboration, "Commissioning of the Particle-flow Event Reconstruction with the first LHC collisions recorded in the CMS detector", *CMS Physics Analysis Summary: PFT-10-001* (2010).

[24] M. Cacciari, G. P. Salam, and G. Soyez, "The anti-kt jet clustering algorithm", *JHEP* **2008** (2008) 063, doi:10.1088/1126-6708/2008/04/063.

[25] CMS Collaboration, "MET performance in 8 TeV data", *CMS Physics Analysis Summary: JME-12-002* (2013).

[26] CMS Collaboration, "CMS Luminosity Based on Pixel Cluster Counting - Summer 2013 Update", *CMS Physics Analysis Summary: LUM-13-001* (2013).

[27] CMS Collaboration, "Determination of Jet Energy Calibration and Transverse Momentum Resolution in CMS", *JINST* **6** (2011) P11002, doi:10.1088/1748-0221/6/11/P11002.

[28] CMS Collaboration, "ECAL Detector Performance, 2011 Data", *CMS Detector Performance Summary: DP-2012-007* (2012).

[29] T. Junk, "Confidence level computation for combining searches with small statistics", *Nucl.Instrum.Meth.* **A434** (1999) 435, doi:10.1016/S0168-9002(99)00498-2, arXiv:hep-ex/9902006.

[30] A. L. Read, "Modified frequentist analysis of search results (the CL_s method)", *CERN-OPEN-2000-205* (2000) doi:10.5170/CERN-2000-005.81.

[31] CMS Collaboration, "Identification of b-quark jets with the CMS experiment", *JINST* **8** (2013) P04013, doi:10.1088/1748-0221/8/04/P04013.

[32] ZEUS Collaboration, "Search for first-generation leptoquarks at HERA", *Phys. Rev. D* **86** (2012) 012005, doi:10.1103/PhysRevD.86.012005.

[33] H1 Collaboration, "Search for first generation leptoquarks in ep collisions at HERA", *Phys. Lett. B* **704** (2011) 388, doi:10.1016/j.physletb.2011.09.017.